International Journal of Steel Structures
March 2014, Vol 14, No 1, 185-194
DOI 10.1007/s13296-014-1016-2

International Journal of
STEEL
STRUCTURES
www.springer.com/journal/13296

Application of Indicial Function for the Flutter Analysis of Long Span Suspension Bridge During Erection

Panot Chobsilprakob[1], Ki-Du Kim[2,*], Songsak Suthasupradit[3], and Anaphat Manovachirasan[4]

[1]*Former Ph.D. Student, Department of Civil and Environmental System Engineering, Konkuk University, Seoul, Korea*
Senior Civil Engineer, Foster Wheeler (Thailand) Limited, Chonburi 20230, Thailand
[2]*Department of Civil and Environmental System Engineering, Konkuk University, Seoul, Korea*
[3]*Center of Excellence for Road and Railway Innovation, Naresuan University, Phitsanulok, Thailand*
Former Ph.D. Student, Dept. of Civil and Environmental System Engineering, Konkuk University, Seoul, Korea
[4]*Department of Civil and Environmental System Engineering, Konkuk University, Seoul, Korea*

Abstracts

The design of cable supported bridge with long span is challenging due to the sensitivity of the dynamic excitation. The aerodynamic instability caused by fluttering can severely affect the safe operation. An application of indicial function to the flutter analysis in time domain is applied to the Great belt East Bridge for both completed and erection stage. The nonlinear least square method was used to extract the aerodynamic indicial parameters for flutter analysis in time domain. The geometric nonlinearity is considered through the nonlinear dynamic analysis. The results showed the good agreement with the wind tunnel test and the validity of the indicial function as well as the important role of the geometrically nonlinear analysis during deck erection.

Keywords: indicial function, time-domain approach, geometric nonlinearity, aero-elastic forces, erection

1. Introduction

The modern long-span bridges have become more flexible and slender, and thus are more susceptible to the dynamic excitation due to wind loads. Aerodynamic instability caused by fluttering can seriously affects to the safe operation of long-span bridge structures. Therefore, flutter instability is major concern in the design of modern long-span bridges. Moreover, the investigation on the long span bridge during erection is also be the importance factor to concern the aerodynamic stability of the bridge especially, in the initial stage of construction which has various factors to reduce the ratio between torsional and vertical frequency.

With the highly nonlinear behavior of the long span bridge, the full time-domain simulation is suggested for both completed and erection stage, this can be done through indicial function load models. Wagner (1925) is the first one who derived the indicial function for thin airfoil theory by expressing the vertical lift force for an instantaneous step change in the up-wind velocity for the single degree of freedom system. Bisplinghoff *et al*. (1955) proposed a general functions for aerodynamic moment and characterized the effects of the different components of the motion on self-excited loads.

The first relevant work of indicial function in bridge application is suggested by Scanlan *et al*. (1974). He applied the airfoil flutter theory and indicial flutter response theory to the bluff structural forms and presented a relationship of flutter derivative and indicial function. Borri and Hoffer (2000) presented a non-stationary aero-elastic load model based on continuous step response function of Wanger-type which is implemented into finite element procedures. Borri *et al*. (2002) include a fading memory into their finite element code for the investigation of aeroelastic instability and for structural analysis in non-linear dynamics. Costa and Borri (2006) further estimated the indicial function coefficients for the stream line and bluff rectangular section through time domain simulation and proved their results with the wind tunnel test. Panot *et al*. (2011), included the effect of material and geometric nonlinearities through the analysis and shown a significant effect of geometric and materials nonlinearity to the aeroelastic instability of the long span bridge.

In this paper, the flutter analysis in time domain

Note.-Discussion open until August 1, 2014. This manuscript for this paper was submitted for review and possible publication on August, 17, 2012; approved on January 13, 2014.

*Corresponding author
Tel: +82-2-2049-6074; Fax: +82-2-452-8619
E-mail: kimkd@konkuk.ac.kr

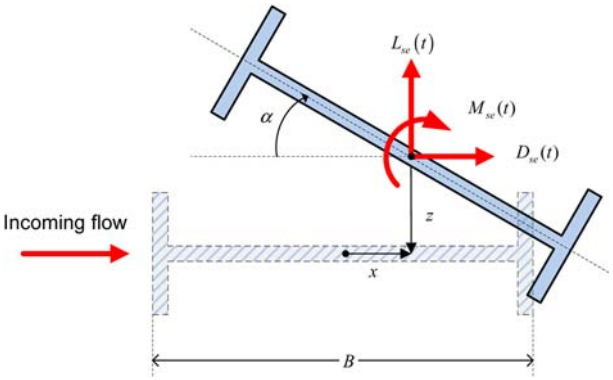

Figure 1. Load model.

through indicial function load model is applied to predict the critical velocity of the Great Belt Bridge during complete state and bridge deck during erection. The model is applied to the geometrically nonlinear analysis. Furthermore, the evolutions of aerodynamic stability limits throughout the deck erection are numerically generated and the results are verified with the wind tunnel test.

2. Self-excited Aerodynamic Force

A classical engineering approach for the flutter problem is the description of self-excited forces in a mixed frequency/time domain formulation via flutter derivatives by Simiu and Scanlan (1986). They assume that the bridge deck possesses uniform properties so that a unit strip with two degrees of freedom can represent the entire bridge. The linearized self-excited aerodynamic forces are determined from the experimentally obtained flutter derivatives. These aerodynamic forces per unit span are related to the heave, sway, and torsional displacements of the bridge deck, as denoted by z, x, α and the associated velocity $\dot{z}$, $\dot{x}$, $\dot{\alpha}$ at the center of elasticity of the deck cross section, which can be expressed as follows:

$$L_{se}(t)=\frac{1}{2}\rho U^2 B\left[KH_1^*\frac{\dot{z}(t)}{U}+KH_2^*\frac{B\dot{\alpha}(t)}{U}+K^2H_3^*\alpha(t)+K^2H_4^*\frac{z(t)}{B}+KH_5^*\frac{\dot{x}(t)}{U}+K^2H_6^*\frac{x(t)}{B}\right] \tag{1}$$

$$D_{se}(t)=\frac{1}{2}\rho U^2 B\left[KP_1^*\frac{\dot{x}(t)}{U}+KP_2^*\frac{B\dot{\alpha}(t)}{U}+K^2P_3^*\alpha(t)+K^2P_4^*\frac{x(t)}{B}+KH_5^*\frac{\dot{z}(t)}{U}+K^2P_6^*\frac{z(t)}{B}\right] \tag{2}$$

$$M_{se}(t)=\frac{1}{2}\rho U^2 B^2\left[KA_1^*\frac{\dot{z}(t)}{U}+KA_2^*\frac{B\dot{\alpha}(t)}{U}+K^2A_3^*\alpha(t)+K^2A_4^*\frac{z(t)}{B}+KA_5^*\frac{\dot{x}(t)}{U}+K^2A_6^*\frac{x(t)}{B}\right] \tag{3}$$

where U=wind velocity; ρ=air mass density; B=bridge deck width; K=reduced frequency with $K=B\omega/U$; ω=circular frequency of response; H_i^*, P_i^*, A_i^* (i=1 ... 6)=dimensionless flutter derivatives determined experimentally from wind tunnel tests.

2.1. Unsteady self-excited force in time domain through indicial function

Chen (2008) said that the self-excited force in time domain by indicial function is an extension of the theory for thin air foil to bluff sections. The response history is expressed as a series of infinitesimal step-wise increments. The non stationary of the evolution in time of the wind load due to the unit displacements is given by indicial aero-elastic function. The wind loads are then given by the convolution integrals of the indicial function with the displacement history.

The indicial functions here are adopted by Salvatori and Spinelli (2006), as

$$L_{se}(t)=qBC_L'\left(\Phi_{Lz}(0)\frac{\dot{z}(t)}{U}+\Phi_{La}(0)\alpha(t)+\int_0^t\left[\dot{\Phi}_{Lz}(t-\tau)\frac{\dot{z}(\tau)}{U}+\dot{\Phi}_{La}(t+\tau)\alpha(\tau)\right]d\tau\right) \tag{4}$$

$$M_{se}(t)=qB^2C_M'\left(\Phi_{Mz}(0)\frac{\dot{z}(t)}{U}+\Phi_{Ma}(0)\alpha(t)+\int_0^t\left[\dot{\Phi}_{Mz}(t-\tau)\frac{\dot{z}(\tau)}{U}+\dot{\Phi}_{Ma}(t+\tau)\alpha(\tau)\right]d\tau\right) \tag{5}$$

where C_L and C_M are the static lift and moment coefficients, respectively, z and α are the vertical and torsional degree of freedom of the bridge deck section, q is dynamic pressure with $q=\frac{1}{2}\rho U^2$, C_L' and C_M' are the slope of lift and moment coefficients, Φ_{ij} (i=L, M; j=z, α) are indicial functions and the dot denote the differentiation with respect to time. The main dimension of the Great Belt suspension bridge is presented in Figure 2.

2.2. Extraction of flutter derivative to indicial functions

Indicial function can be considered in two parts: The

constant part, a_{0hk}, accounts for quasi-steady effect, and the second part, n exponential group of, a_{ihk}, b_{ihk}, describe the unsteady evolution of the force, where $s = Ut/b$ is the dimensionless time, as expressed by the following equation.

$$\Phi_{hk}(s) = a_{0hk} - \sum_{i=1}^{n} a_{ihk} \exp(-b_{ihk} s) \tag{6}$$

The experimental procedures to obtain the indicial function are not yet widely established in contrast with the aero-elastic derivative. However, it is possible to obtain an indicial function from aero-elastic derivative. The usual relationship among flutter derivative and indicial functions are illustrated by Borri, C., Costa, C., Zahlten, W., (2002); below,

$$\begin{aligned}
&\frac{2\pi}{U_{red}} H_1^* = \frac{dC_L}{d\alpha}\left[1 - \sum_{i=1}^{n} a_{iLz} \frac{\pi^2}{b_{iLz}^2 U_{red}^2 + \pi^2}\right],\\
&\frac{2}{U_{red}^2} H_4^* = \frac{dC_L}{d\alpha}\left[\sum_{i=1}^{n} a_{iLz} \frac{b_{iLz}}{b_{iLz}^2 U_{red}^2 + \pi^2}\right],\\
&\frac{4\pi}{U_{red}^3} H_2^* = \frac{dC_L}{d\alpha}\left[\sum_{i=1}^{n} -a_{iL\alpha} \frac{b_{iL\alpha}}{b_{iL\alpha}^2 U_{red}^2 + \pi^2}\right],\\
&\frac{4\pi^2}{U_{red}^2} H_3^* = \frac{dC_L}{d\alpha}\left[1 - \sum_{i=1}^{n} a_{iL\alpha} \frac{\pi^2}{b_{iL\alpha}^2 U_{red}^2 + \pi^2}\right],\\
&\frac{2\pi}{U_{red}} A_1^* = \frac{dC_M}{d\alpha}\left[1 - \sum_{i=1}^{n} a_{iMz} \frac{\pi^2}{b_{iLz}^2 U_{red}^2 + \pi^2}\right],\\
&\frac{2}{U_{red}^2} A_4^* = \frac{dC_M}{d\alpha}\left[\sum_{i=1}^{n} a_{iMz} \frac{b_{iMz}}{b_{iMz}^2 U_{red}^2 + \pi^2}\right],\\
&\frac{4\pi}{U_{red}^3} A_2^* = \frac{dC_M}{d\alpha}\left[\sum_{i=1}^{n} -a_{iM\alpha} \frac{b_{iL\alpha}}{b_{iM\alpha}^2 U_{red}^2 + \pi^2}\right],\\
&\frac{4\pi^2}{U_{red}^2} A_3^* = \frac{dC_M}{d\alpha}\left[1 - \sum_{i=1}^{n} a_{iM\alpha} \frac{\pi^2}{b_{iM\alpha}^2 U_{red}^2 + \pi^2}\right],
\end{aligned} \tag{7}$$

Derivative of aerodynamics coefficient with respect to the angle of attack are in principle different from the thin airfoil. Therefore, a nonlinear least square method is applied to identify the indicial function coefficients from the experimental aero-elastic derivative. Since the indicial function must converge into one as time approaches infinity, the parameter b_{ihk} in indicial functions must be a positive value.

3. Flutter Analysis of the Great Belt East Bridge

The modern suspension bridges are flexible and slender which have the potential to be susceptible to the dynamic excitation due to wind-induced instabilities. Aerodynamic instability due to fluttering is one of the serious effects for the safe operation of long span bridge structures. Agar (1989) said that flutter occurs at the certain wind speed which causes the aerodynamic forces acting to the oscillating structures, so inducing the vibration. The self-excited oscillation motion of long span bridges is the most significantly related to the lowest heave and torsional modes of bridges. Therefore, flutter instability is concerned in the design of the modern long span bridge.

Weight (2009) presented that the Great Belt East Bridge is one of the longest suspension bridges located in Denmark. The completed east bridge has a central span of 1,624 m and side span of 535 m. The bridge was opened for traffic on 1998. The bridge deck is a 31 m wide and about 4 m deep steel box. This girder is continuous over the full cable supported length of 2,694 m. The form of the box girder is streamlined to resist the aerodynamic instability due to the strong wind. The ratio of cable sag to main span length was chosen to be 1/9. The main cables are fixed through stiffening girder at the mid span. The total height of the concrete pylons, including cable and cable saddle, is approximately 258 m. The bridge geometries are given in Fig. 2 and their properties are given in Table 1.

3.1. Frequency analysis and calculation of the Rayleigh damping ratio

Modeling of the Great Belt suspension bridge can be done using a combination of appropriate elements. The single spine girder model is used to model the deck which is suitable for the model of single-cell box girder bridges. The suspension cables are connected to the spine through

Table 1. Geometries and material properties of the Great Belt suspension bridge (Karoumi, 1999; Kim *et al*., 2002)

Member.	E (GPa)	A (m^2)	I_t (m^4)	w (kN/m)
Deck	210	1	3.32	144.8
Main span cable	210	0.40	-	32.9
Side span cable	210	0.41	-	33.8
Hanger	210	0.025	-	-
Pylon (0-75.5 m)	40	37.5	750	882.4
Pylon (75.5-136.2 m)	40	32.5	275	764.4
Pylon (136.2-196.9 m)	40	30.0	200	705.6
Pylon (196.9-257.6 m)	40	25.0	150	588.0

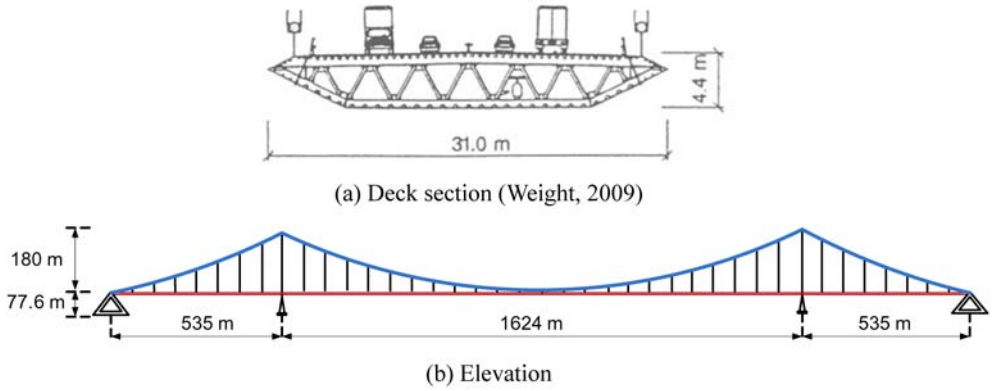

Figure 2. Main dimension of the Great Belt suspension bridge.

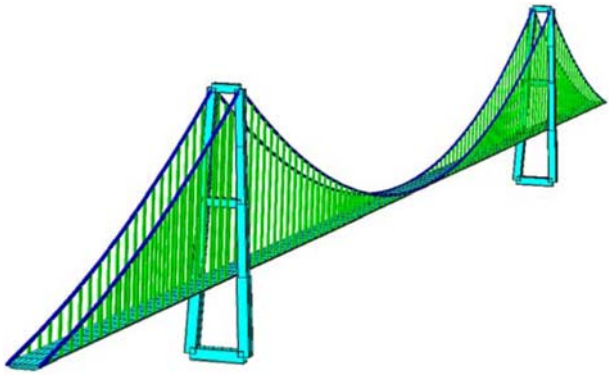

Figure 3. Finite element model of The Great Belt Bridge.

rigid link element. The cable element which considering the geometric nonlinearity is used to model the suspension cable. The profile of a suspension cable under its own weight is optimized through the shape-finding process.

The main span of the bridge is discretized in to 112 frame elements. The bridge girder is supported every 24 meters by pair of hangers. The natural frequency as well as their corresponding mode shapes are given in -. The heave and torsional motions of the bridge deck are must be prioritized when dealing with the wind stability of the bridge. The frequency of the fundamental mode which corresponds to motion induced force is 0.106 Hz. This is equivalent to a 1st vertical mode.

The structural behavior is a combination of cable and frame in which a vertical resistance of the system is the one of a cable with negligible the flexural rigidity. Horizontal and torsional stiffness is the same as a frame with rectangular cross section embedded at the ends. The structural behavior is a combination of cable and frame in which a vertical resistance of the system is the one of a cable with negligible the flexural rigidity. Horizontal and torsional stiffness is the same as a frame with rectangular cross section embedded at the ends. lists the first three

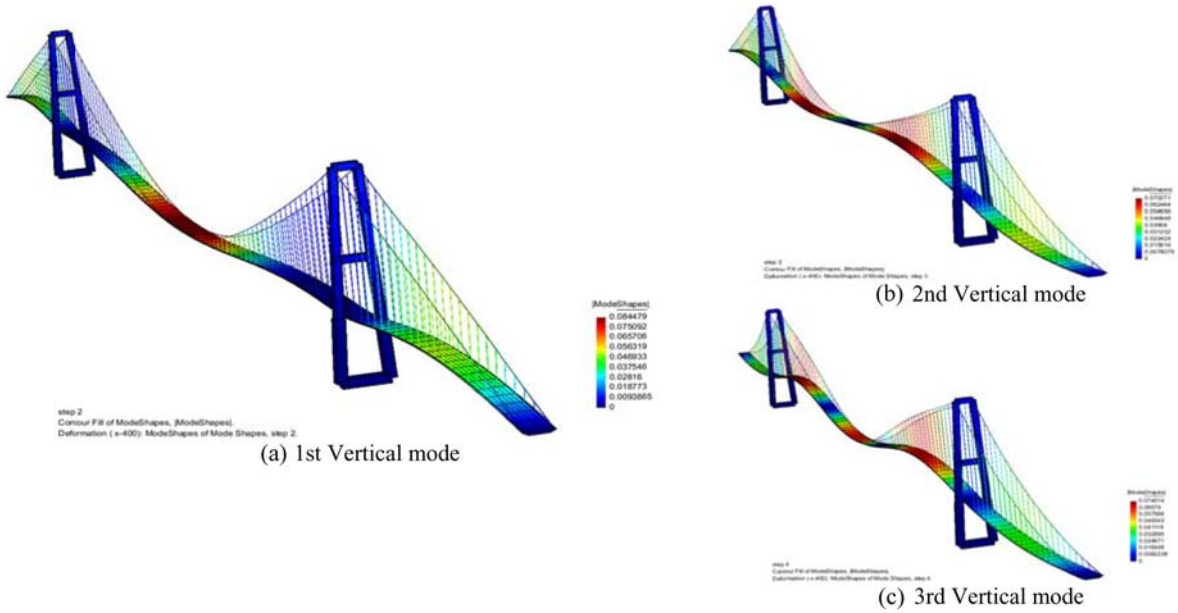

Figure 4. Vertical mode of the Great Belt Bridge.

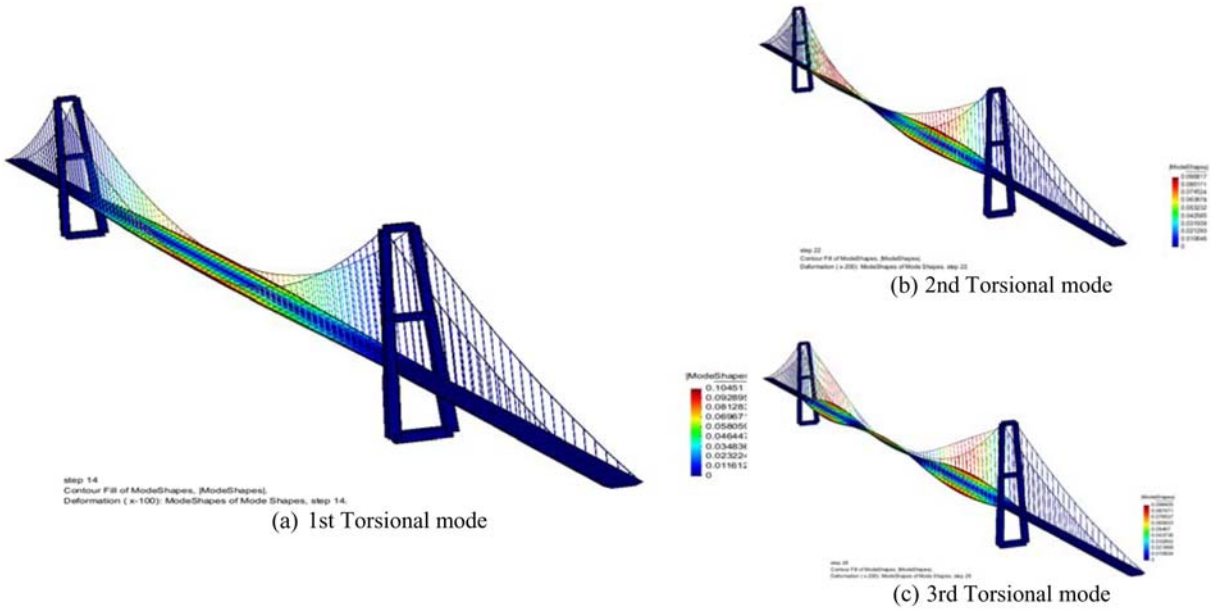

Figure 5. Torsional mode of the Great Belt Bridge.

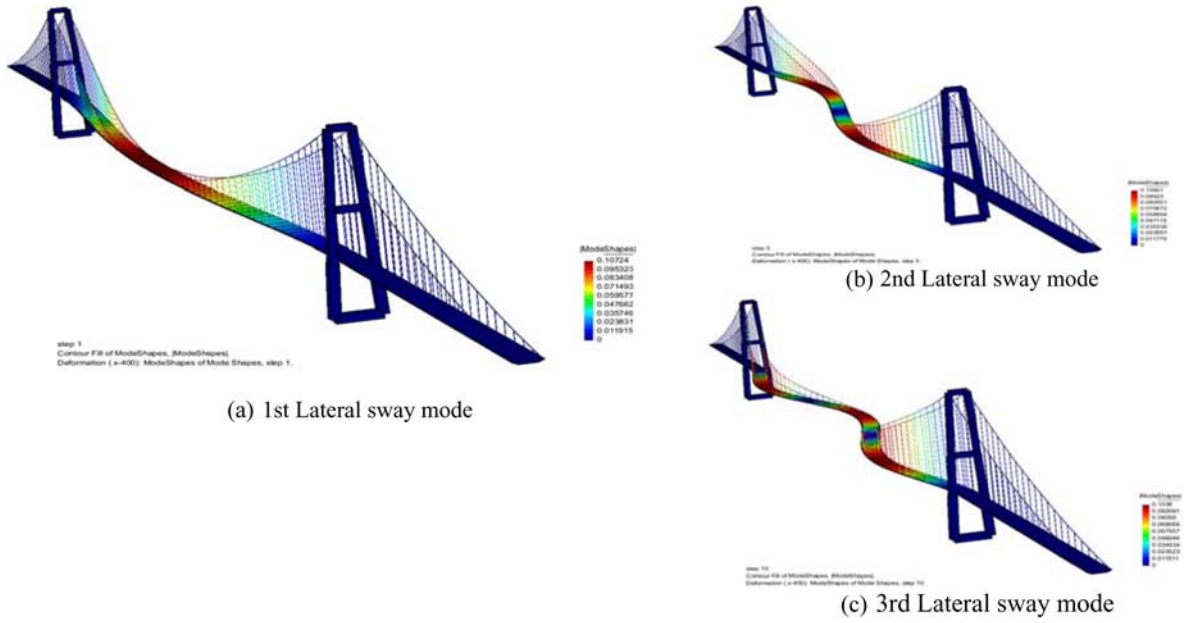

Figure 6. Lateral sway mode of the Great Belt Bridge.

fundamental modes corresponding to the vertical, torsional, and lateral modes severally. The analytical results are estimated using XFinas (Kim, 2007) software. Subspace iteration method is used in the Eigenvalue analysis. These values are relatively accurate comparing to the corresponding experimental values given by Larsen and Jacobsen (1992).

Rayleigh damping ratio of 0.2% is assigned considered the first vertical and first torsional modes as the calculation of Rayleigh damping which are given below:

$$[C]=\alpha_r\ [M]+\ \beta_r\ [K] \tag{8}$$

where $[C]$ is the structural damping matrix, $[M]$ is the mass matrix, $[K]$ the stiffness matrix, α_r and β_r are Rayleigh damping constants.

The symmetric vertical and torsional mode, corresponding to the natural frequency of ω_h =0.666 rad/s and ω_α =1.954 rad/s according to the Eigenvalue analysis results, are likely to participate in the oscillation in the case of flutter instability. The damping ratio of both two modes is $\zeta_h=\zeta_\alpha$=0.2%.

The Rayleigh damping coefficient is calculated as:

$$\zeta_n=\frac{\alpha_r}{2}\frac{1}{\omega_n}+\frac{\beta_r}{2}\omega_n \tag{9}$$

Table 2. Modal period and shape

Mode	Frequency (Hz) (Current)	Analytical (Larsen, 2003) Frequency (Hz)	Experimental (Larsen and Jacobsen, 1992) Frequency (Hz)	Mode shape
2	0.106	0.100	0.997	1st vertical
3	0.115	0.115	0.115	2nd vertical
4	0.132	0.135		3rd vertical
14	0.310	0.278	0.289	1st Torsional
20	0.414	0.383	0.391	2nd Torsional
24	0.542	0.502		3rd Torsional
14	0.059	0.052	0.0523	1st Lateral
20	0.141	0.123	0.127	2nd Lateral
24	0.246	0.187		3rd Lateral

Substituted the natural frequency, ω_h=0.666 rad/s and ω_α=1.954 rad/s to Eq. (9) would result in α_r=0.001987 and β_r=0.001527 respectively. Therefore, the structural damping matrix during the time domain analysis is:

$$[C]=0.001987\ [M]+0.001527\ [K] \quad (10)$$

3.2. Aerodynamic derivative

The aerodynamic derivatives were conducted by Timothy (1992), from the section model tests. Furthermore, the experimental aerodynamic derivative for the heaving and rotation are given in Figs. 7 and 8, respectively. The nonlinear least square fit is then performed to evaluate the indicial function parameters which are agree well with the experimental aerodynamic derivative.

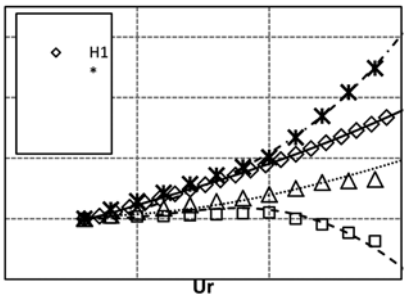

Figure 7. Approximation of experimental derivative of the great belt bridge H_i^* (i=1,..,4) by indicial function.

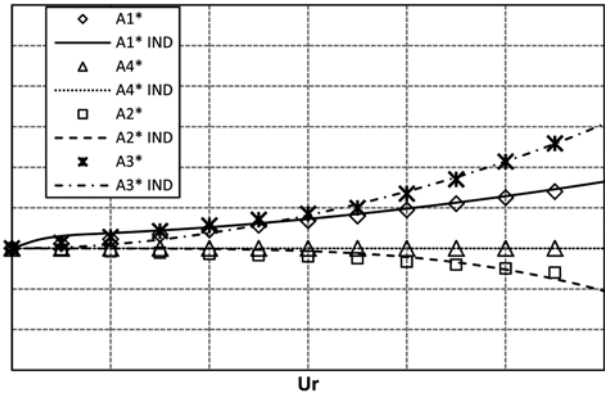

Figure 8. Approximation of experimental derivative of the great belt bridge A_i^* (i=1,..,4) by indicial function.

3.3. Flutter analysis in Time domain during completed state

Based on the indicial function parameters obtained earlier, the flutter analysis in time domain is performed

Table 3. Critical velocity of idealized suspension bridge

Type of test	Flutter Velocity U_{cr} (m/s)
Section model (Experimental)	70-74
Taut strip (Experimental)	72
Full bridge (Experimental)	70-75
Current flutter analysis (3D FEM)	73

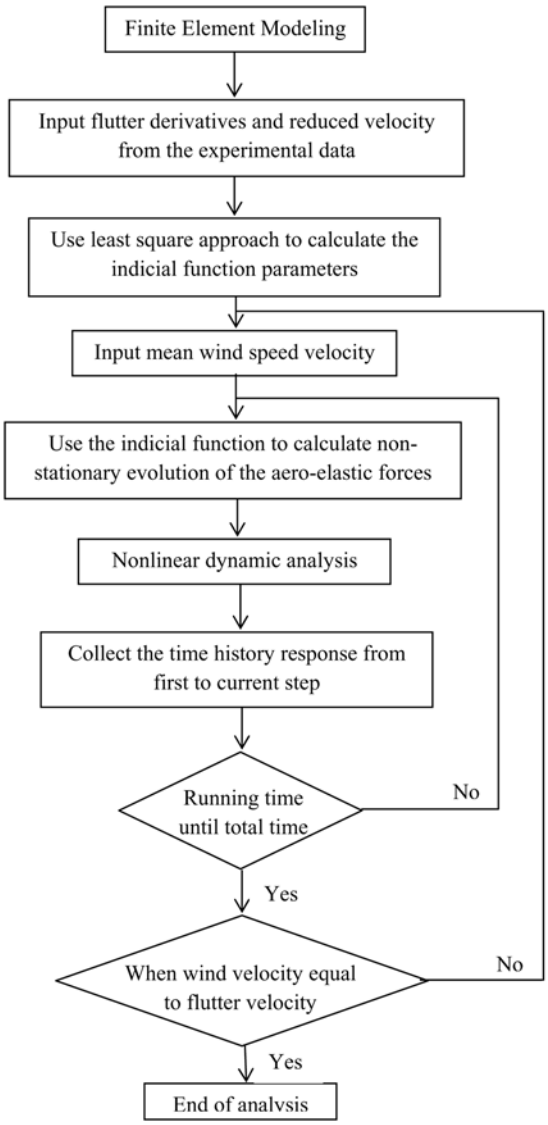

Figure 9. Flutter analysis flow chart.

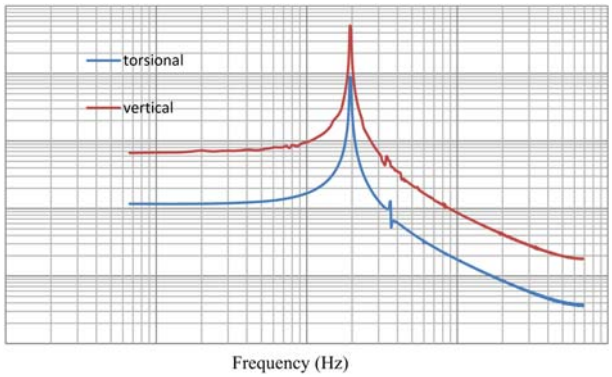

Figure 10. Flutter frequency for torsional and vertical DOF.

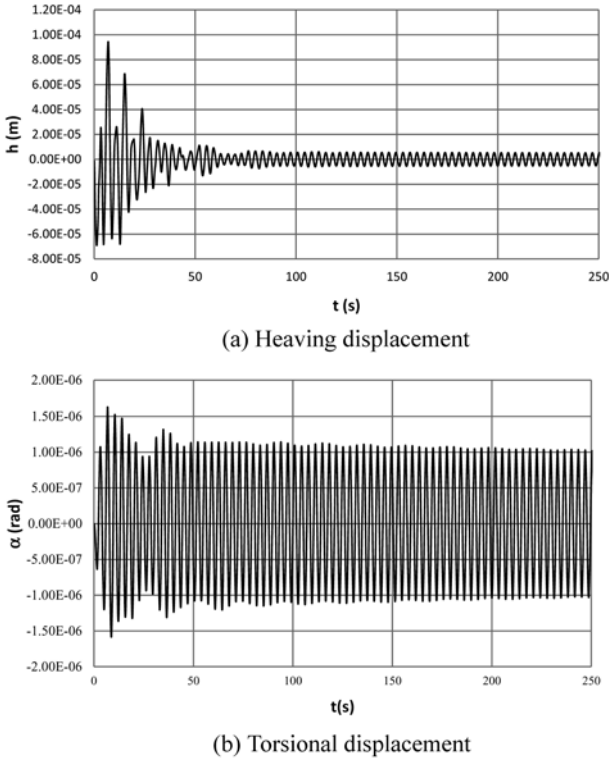

Figure 11. Time-histories of motion at a subcritical wind velocity U=70 m/s.

through a convolution integral and entails a step by step dynamic finite element method where the aero-elastic forces are adopted. The present model is implemented into XFINAS (Kim, 2007) developed by the Konkuk University. The flow chart of the algorithm is shown in Fig. 9. In addition, the time histories of the responses are shown in Figs. 10-12. It can be seen that, the structural system is still damped at a wind velocity of 70 m/s as shown in Fig. 10.

A flutter condition is obtained at a critical velocity A= 73.0 m/s (Fig. 11), with a flutter frequency f=0.193 Hz. The results are agreed well to the wind tunnel test given by Larsen and Jacobsen (1992) as shown in Table 3.

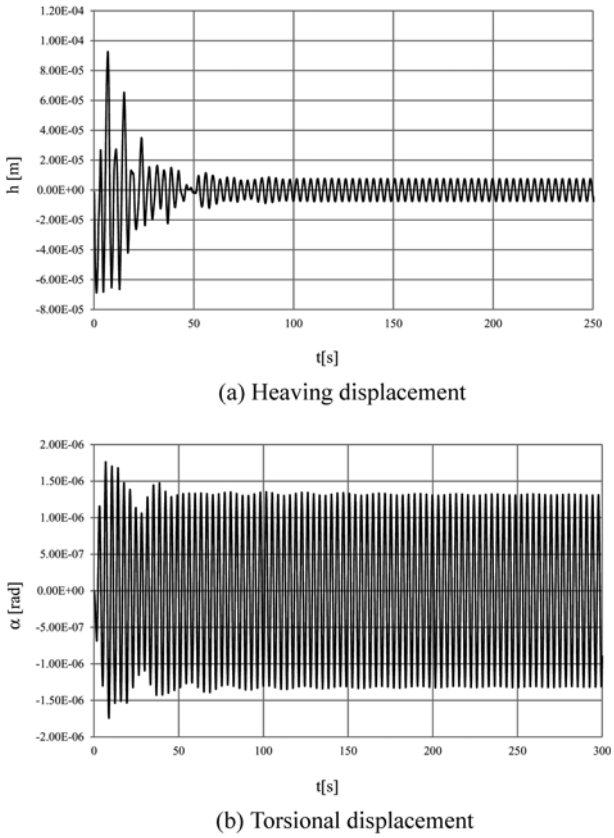

Figure 12. Time-histories of motion at a critical wind velocity U=73 m/s.

It should be pointed out that the frequencies of the responses are coincided in both torsional and heaving displacement (Fig. 10). This characteristic is referred as a coupled flutter, which in general occurred for the streamed line sections.

With the greater incoming wind velocity, the structure is unable to damp the energy from the self-excited force hence; the amplitude of vertical and rotation are diverged as shown in Fig. 13.

3.4. Aero-elastic stability analysis during erection

During erection of suspension bridges a number of aerodynamic problem are encountered which relate to the fact that the bridge structure is incomplete, thus various structural components do not receive the conditions as intended in the complete structure.

Erection of the suspension bridge may proceed in a number of different ways. The deck erection of a suspension bridge involved many challenging problems with respect to both construction safety and time schedules. In general, deck erection sequences of suspension bridges can be classified into the following three types: (1) mid span to pylons; (2) pylons to mid span; and (3) four working fronts.

The mid span to pylon approach was selected for the Great Belt East during erection. The critical damping

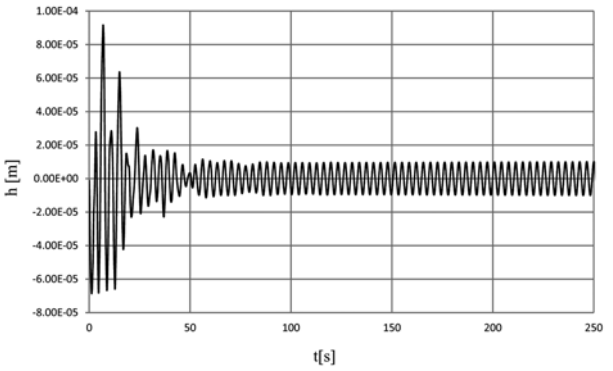

(a) Heaving displacement

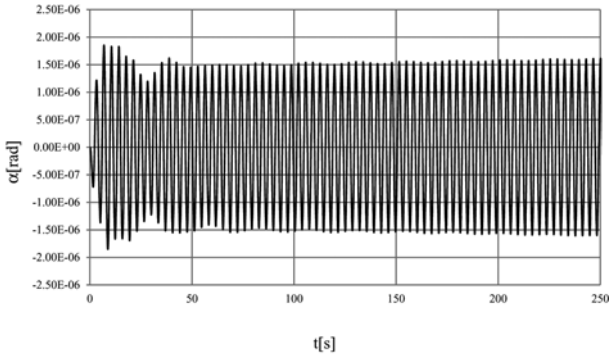

(b) Torsional displacement

Figure 13. Time-histories of motion at a super critical wind velocity U=73 m/s.

Table 4. Comparison of Critical flutter velocity during erection

% of erection	U_c (Larsen and Jacobsen, 1992)	U_c (Current)
23	34.8	38.5

ratio considered during the erection is 0.01. It's observed from the analytical results that the stability limit of the bridge during 20% of erection is 38.5 m/s and give a good agreement with the analytical results 34.8 m/s performed by Larsen and Jacobsen (1992).

The parametric studies for the various erection stages of the Great Belt Bridge are performed afterward. The geometrically nonlinear is considered and the results are compared with the linear analysis and wind tunnel test (Danish, 1997). Introducing the structural damping ratio of 0.002 for the final section which is the same value applied to the full bridge model. The results can be obtained as shown in Fig. 16. We can conclude the analysis results as follows:

(1) In the initial stage of construction, the critical flutter speeds is very high. The main reason is that the bridge span is still short under the erection; therefore, the mass is contributed to vibration due to main cables. This mean the inertia force is still large compared to the aerodynamic excitation which is caused by the short deck.

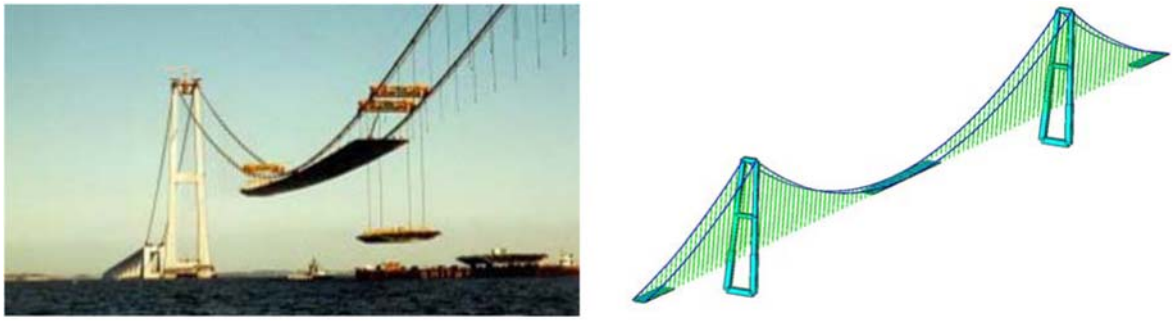

(a) Erection process of the Great Belt East bridge (b) Finite element model

Figure 14. (a) Erection process of the Great Belt East bridge (b) Finite element model.

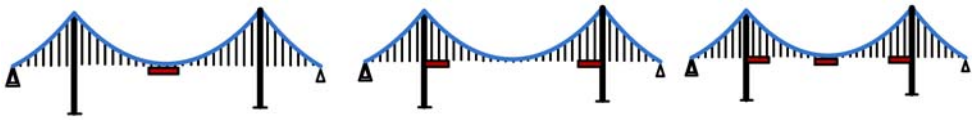

(a) Midspan to Pylons (b) Pylons to Midspan (c) Four working Fronts

Figure 15. Deck erection sequence.

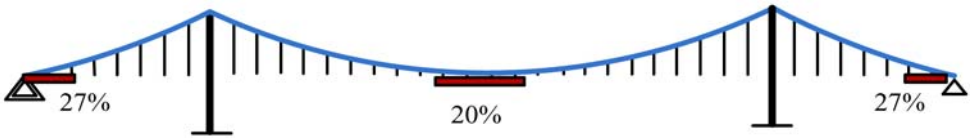

Figure 16. Verification problem.

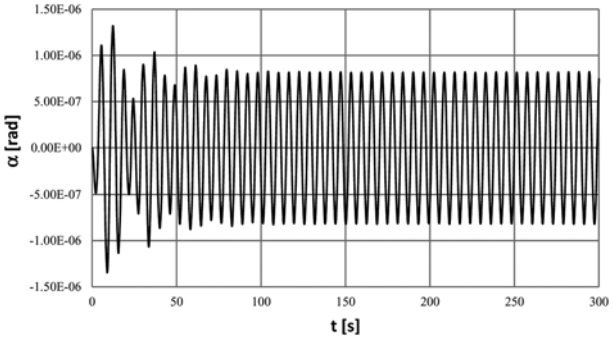

Figure 17. Critical wind velocity (20% of erection) U = 38.5 m/s.

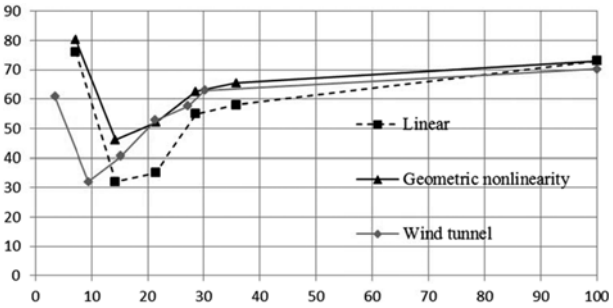

Figure 18. Stability limits of The Great Belt East Bridge during Erection.

(2) The stability limit is lower through the first half of the erection period. The reason is the lack of overall torsional stiffness. The bending stiffness, on the other hand, is less sensitive to the degree of deck erection, since most of the bending stiffness if provided by the main cables.

(3) The critical flutter speed becomes lowest at a relatively early stage, i.e., about 20% of the deck erection. At this point, the deck is already long enough to pick up the excitation force and it does not give enough structural stiffness.

(4) The results from the linear analysis tend to overestimate the critical velocity especially during the first half of the erection whereas the stiffness of the system is not completely developed. Therefore, the geometrically nonlinear is recommended for the aero-elastic stability analysis of the deck during erection

4. Concluding Remarks

The flutter analysis in time domain using indicial function is a major concern in modern long span bridge design, which was applied to the Great belt East Bridge for both completed and erection stage. The flutter analysis in time domain simulation was developed by the finite element technique with the indicial function. The geometric nonlinearity was considered through the nonlinear dynamics analysis. The approaches include the frequency and time integration analysis in the complete and erection stages. The analysis results had shown a good agreement with the wind tunnel test for both stages. The analysis results also showed the important role of the geometrically nonlinear analysis during deck erection and therefore, useful to improve the aerodynamics performance of the structure during erection in additional to the experimental predicting of the flutter limit.

Acknowledgments

This work was supported by the Konkuk University.

Nomenclature

A	: cross section area of structural components
A_i^* (i=1...6)	: frequency-dependent flutter derivatives
a_0	: indicial function coefficient
i_{ihk}	: indicial function coefficient
b_{ihk}	: indicial function coefficient
B	: Bridge deck width
C_{L_t}	: static lift coefficient
C_L	: slope of lift coefficient
C_M	: static moment coefficient
C_M	: slope of moment coefficient
D_{se}	: aeroelastic drag force per unit length
f_{cr}	: flutter frequency
f_z	: vertical frequency
f_α	: torsional frequency
H_i^* (i=1...6)	: frequency-dependent flutter derivatives
I_t	: mass moment of inertia per unit length
K	: reduced frequency
L_{se}	: aeroelastic lift force per unit length
m	: mass per unit length
M_{se}	: aeroelastic moment per unit length
P_i^* (i=1...6)	: frequency-dependent flutter derivatives
q	: dynamic pressure
s	: dimensionless time
t	: time
U	: mean wind velocity in the main flow direction
U_{cr}	: flutter velocity
U_{red}	: reduced velocity
w	: weight per unit length
x	: sway displacement
$\dot{x}$	: sway velocity
z	: vertical displacement
$\dot{z}$	: vertical velocity
Δt	: time step incremental

Greek letters

Φ_{ij}	: indicial functions
ρ	: air mass density
ω	: circular frequency
ω_z	: vertical circular frequency
ω_α	: torsional circular frequency
ξ_z	: structural damping ratio in vertical mode
ξ_α	: structural damping ratio in torsional mode
α	: torsional displacement

$\dot{\alpha}$: torsional velocity
α_r, β_r : Rayleigh damping parameters

References

Agar, T. J. A. (1989). "Aerodynamic flutter analysis of suspension bridge by a modal technique." *Energ. Struct.*, 11, pp. 75-82.

Bisplinghoff, R. L., Ahley, H., and Halfman, R. L. (1955). *Aeroelasticity*. Dover Publication, Inc., Mineola, New York.

Borri, C., Costa, C., and Zahlten, W., (2002). "Non-stationary flow forces for the numerical simulation of aeroelastic instability of bridge decks." *Comput. Struct*, 80, pp. 1071-1079.

Borri, C. and Hoffer, R. (2000). "Aeroelastic wind forces on flexible girders." *Meccanica*, 35(10), pp. 1-15.

Chen, X., Matsumoto, M., and Kareem, A. (2000) "Time domain flutter and buffeting response analysis of bridges." *Journal of Engineering Mechanics*, 126(1), pp. 7-16.

Costa, C. and Borri, C. (2006). "Application of indicial functions in bridge deck aeroelasticity." *J. Wind Eng. Ind. Aerodyn.*, 94, pp. 859-881.

Karoumi, R., (1999). "Some modeling aspects in the nonlinear finite element analysis of cable supported bridges." *Computer and Structures*, 71, pp. 397-412.

Kim, H. K. and Lee, M. J. (2002.) "Nonlinear shape-finding analysis of a self-anchored suspension bridge." *Engineering Structures*, 24, pp. 1547-1559.

Larsen, A. and Jacobsen, S. (1992). "Aerodynamic design of the Great Belt East bridge." *Proc. First International Symposium on Aerodynamics of Large Bridges*, Copenhagen, Denmark.

Larsen, A. (2003). "Aerodynamic aspects of the final design of the 1624 m suspension bridge across the Great Belt." *J. Wind Eng. Ind Aerodyn*, 48, pp. 261-285.

Panot, C., Songsak, S., and Kim, K. D. (2011). "Aeroelastic analysis of long span bridges via indicial functions considering geometric and material nonlinearity." *International Journal of Steel Structures*, 11(2), pp. 215-226.

Salvatori, L. and Spinelli, P., (2006). "Effects of structural nonlinearity and along-span wind coherence on suspension bridge aerodynamics: Some numerical simulation results." *J. Wind Eng. Ind. Aerodyn*., 94, pp. 415-430.

Scanlan, R. H., Béliveau, J. G., and Budlong, K. (1974). "Indicial aerodynamics functions for bridge decks." *Journal of Engineering Mechanics*, 100, pp. 657-672.

Simiu, E. and Scanlan, R. H. (1986). *Wind Effects on Structures*. Wiley, New York.

Timothy, A. R. (1992). "Wind tunnel test for the Great Belt link." *Proc. First International Symposium on Aerodynamic of Large Bridges*, Copenhagen, Denmark.

Wagner, H., (1925). On the origin of the dynamic buoyancy of wings. ZAMM 5, *Aeronautics Twentieth Annual Report of the National Advisory Committee for Aeronautics*, pp. 17-35.

Weight, A. J. (2009). "Critical analysis of the Great Belt East bridge, Denmark." *Proc. Bridge Engineering 2nd Conference*, University of Bath, Bath, UK.

Kim, K. D. (2007). XFINAS 3.0. Theory, Example, Reference and User Manual. Report No. 6, Department of Civil and Environmental Engineering, Konkuk University, Korea.